Molecular-dynamics simulation of amorphous alloys. I. Atomic structure of fully relaxed systems

1989 J. Phys.: Condens. Matter 1 9985

(http://iopscience.iop.org/0953-8984/1/50/002)

J. Phys.: Condens. Matter 1 (1989) 9985–10001. Printed in the UK

Molecular-dynamics simulation of amorphous alloys: I. Atomic structure of fully relaxed systems

E H Brandt
Max-Planck-Institut für Metallforschung, Institut für Physik, D-7000 Stuttgart 80, Federal Republic of Germany

Received 10 October 1988, in final form 25 April 1989

Abstract. Amorphous structures of one or two types of atoms of various radii and masses and interacting by various central potentials are simulated by molecular dynamics on a computer. Fully relaxed atomic arrangements resulting from simulated annealing are investigated with the aim of getting an indication of possible mechanisms of self-diffusion, which is quantitatively studied in the following paper. Relaxation of random positions yields dense and homogeneous amorphous structures with neither microcrystals nor holes. Defective crystals, depending on the annealing rate and potentials, yield either defective crystals again or completely amorphous structures, which in some cases contain holes or channels.

1. Introduction

Self-diffusion of the atoms in solids is an interesting statistical problem. Whereas much is known about diffusion mechanisms in crystalline solids, diffusion in non-crystalline solids is still not well understood (Kronmüller and Frank 1989 and references therein). Concepts like diffusion via vacancies or interstitials or along grain boundaries, which have proven very useful in crystalline matter, usually cannot be applied to amorphous alloys because the notion of such defects loses its sense, or at least has to be considered, in closely packed amorphous arrangements of atoms. Extended or smeared-out defects like regions of slightly higher or lower densities, which at low temperatures T prove to be stable (Brandt and Kronmüller 1983, Brandt 1984) cannot migrate without self-destruction. This is a general feature of any statistically (i.e. at $T = 0$) stable configuration with internal stresses in amorphous alloys like density fluctuations or quasi-dislocations. Such defects may disappear when T is raised (Laakkonen and Nieminen 1988) or when the surrounding atoms rearrange.

Generally speaking, the definition of defects in amorphous alloys presents problems. In order to be a useful concept, (i) a defect should satisfy some conservation law and (ii) there should be far fewer defects than atoms. These two conditions are satisfied in crystals. (i) For example, dislocations cannot end inside the crystal and vacancies or interstitials cannot vanish except by reaction with other defects or with the surface. In amorphous metals, however, regions of 'free volume' (reduced atomic density) can disappear inside the bulk like a hole collapses in a sand heap. In particular, these regions do not have to migrate to the surface as is sometimes believed. (ii) It is the scarcity of defects which makes the description of a real crystal as a perfect crystal with defects a useful concept (Seeger 1955, 1958). In amorphous solids the concentration of appropriately defined local 'defects' is comparable to the concentration of atoms; this renders

0953-8984/89/509985 + 17 $02.50

the concept of such structural defects of little help. The definition of more extended defects appears to be more sensible. For example, dipolar stress fields ascribed to dislocation-like sources were concluded from magnetisation curves of amorphous ferromagnets (Kronmüller and Ulner 1977, Kronmüller *et al* 1979). The quasi-dislocation loops predicted by Kronmüller *et al* (1979) were observed by Piller and Haasen (1982) by an atom-probe field-ion microscope and identified as pinning centres in amorphous superconductors by Wördenweber *et al* (1988).

Various microscopic mechanisms have been proposed for self-diffusion in amorphous alloys (Frank *et al* 1988), e.g. direct diffusion, diffusion by collective motion of many neighbouring atoms, by vacancy mechanisms, or along 'easy channels' where the atomic density is less than average. Evidence for the latter mechanism is concluded from the experimental observation (Horváth *et al* 1987, 1988) that the diffusivity decreases when the amorphous specimen is annealed. The self-diffusion data obtained by these radiotracer experiments are reviewed and analysed by Kronmüller and Frank (1989).

In order to get more insight into this problem we performed molecular-dynamics simulations. In the present paper (part I) we describe the numerical method (§ 2) and characterise the resulting amorphous structures by their radial density functions (§ 3) and by plots of the atomic positions (§ 4) which visualise the arrangement of nearest neighbours and show dilute regions, holes or empty channels. In § 5 the influence on relaxed random structures of the type of interaction (atomic size and softness), of the annealing velocity and of the initial (e.g. random) atomic arrangement is studied. In § 6 a strongly perturbed FCC crystal is chosen as initial atomic arrangement. In this case, depending on the interaction and on the relaxation method or velocity, either another defective FCC crystal results (with narrow peaks in the radial density) or a completely amorphous arrangement. Section 7 summarises the results. A forthcoming paper (part II, Brandt 1989) deals with the paths of oscillating and diffusing atoms and presents quantitative results of diffusion coefficients and their temperature dependence.

2. The simulation method

Our model system contains N_A atoms A of mass m_A and $N_B < N_A$ atoms B of mass m_B with positions $\boldsymbol{r}_i$ in a cube with periodic boundary conditions. The volume and pressure can thus be controlled without introducing a surface. The atoms interact by central symmetric pair potentials $\phi_{AA}(r)$, $\phi_{AB}(r)$ and $\phi_{BB}(r)$ with repulsive core and attractive tail. The position of their minima $d_{AA} = 2r_A$ and $d_{AB} = r_A + r_B$ define the atomic radii r_A and r_B. The interaction ϕ_{BB} is chosen to be merely repulsive to ensure good separation of the B-type atoms.

The use of pair potentials is the main restriction of our model. This may be improved by using the empirical density-dependent potentials constructed by Daw and Baskes (1983, 1984), Finnis and Sinclair (1984) or Ackland *et al* (1987). In order to stress the model character of pair potentials for solids we chose simple parabolae (Brandt 1985, Brandt and Kronmüller 1987) which look similar to Morse potentials cut off at $r = R$ (figure 1):

$$\phi_1(r) = a(u^4 + u^2)$$

$$lv_2(r) = a(u^4 - 2u^2)$$

$$\phi_3(r) = \tfrac{1}{2}a(u^6 - 3u^2)$$

$$u = (R - r)/(R - r_0) \qquad r < R$$

$$u = 0 \qquad r \geqslant R.$$

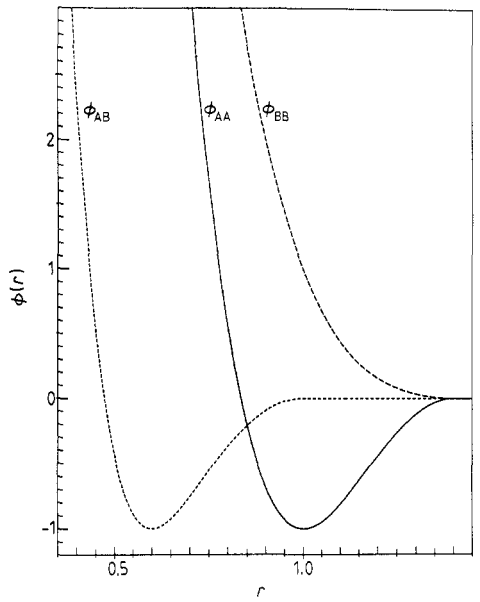

Figure 1. The three interaction potentials defined by equation (1): $\phi_{BB}(r) = \phi_1(r)$ $(a = 0.5, r_0 = 1, R = 1.4)$; $\phi_{AA}(r) = \phi_2(r)$ $(a = 1, r_0 = 1, R = 1.4)$; $\phi_{AB}(r) = \phi_3(r)$ $(a = 1, r_0 = 0.6, R = 1)$. Same potentials as in figure 3 below.

The monotonically decreasing function ϕ_1 is used for ϕ_{BB}. For ϕ_{AA} and ϕ_{AB} we use ϕ_2 or ϕ_3, which exhibit minima of depth a at $r = r_0$ where $u = 1$. The function $\phi_3(r)$ exhibits a sharper minimum than $\phi_2(r)$. In the following we write d_{AA}, d_{AB} or d_{BB} for r_0; R_{AA}, R_{AB} or R_{BB} for R; and a_{AA}, a_{AB} or a_{BB} for a.

One aim of the present paper is to investigate the dependence of the properties of the amorphous model system on the depths and ranges of the interaction potentials. In order to bring this dependence out more clearly, we choose as energy and length unit the depth and position of the minimum in $\phi_{AA}(r)$ and as mass unit m_A. This choice defines also the units $\hat{t}$ of time and $\hat{D}$ of diffusivity. Thus in the following we put

$$\begin{aligned} &d_{AA} = 2r_A = 1 \\ &-\phi_{AA}(d_{AA}) = a_{AA} = U_A = 1 \\ &m_A = 1 \\ &\hat{t} = 2r_A(m_A/U_A)^{1/2} = 1 \\ &\hat{D} = 2r_A(U_A/m_A)^{1/2} = 1. \end{aligned} \tag{2}$$

The essential parameters of the model system are then R_{AA}, d_{AB}, a_{AB}, d_{AB}, R_{AB}, a_{BB}, d_{BB}, R_{BB}, m_B and N_B/N_A. The potential and kinetic energies of this system read

$$U_{pot} = \tfrac{1}{2} \sum_{\substack{i=i_A \\ i\neq j}} \sum_{j=j_A} \phi_{AA}(r_{ij}) + \sum_{i=i_A} \sum_{j=j_B} \phi_{AB}(r_{ij}) + \tfrac{1}{2} \sum_{\substack{i=i_B \\ i\neq j}} \sum_{j=j_B} \phi_{BB}(r_{ij}) \tag{3}$$

$$U_{kin} = \tfrac{1}{2} m_A \sum_{i=i_A} \dot{r}_i^2 + \tfrac{1}{2} m_B \sum_{i=i_B} \dot{r}_i^2. \tag{4}$$

Here r_i are the positions of the A-type atoms $(i = i_A)$ or B-type atoms $(i = i_B)$ and $r_{ij} = |r_i - r_j|$. For ideal FCC or HCP lattices with pure nearest-neighbour interaction, one has $U_{pot} = -6N$. The same binding energy approximately holds also for our

Table 1. Potential energy referred to the ideal FCC value and coordination number Z of fully relaxed amorphous systems of $N = N_A = 100$ atoms with interaction ranges $R_{AA} = 1.5$ (soft) to $R_{AA} = 1.2$ (hard). The upper six rows give results of three runs with different annealing velocities and constant volume (see text). In the lower three rows also the volume was relaxed resulting in an expansion ($d_0 > d_{AA}$) or contraction ($d_0 < d_{AA}$) of the system.

	Interaction range, R_{AA}						
	1.5	1.4	1.3	1.25	1.2	C_{vel}	N_{rel}
Energy, $U_{pot}/6NU_A$	−1.0113	−0.9252	−0.8757	−0.8259	−0.7622	0.995	2000
	−1.0088	−0.9482	−0.8709	−0.8194	−0.7485	0.990	1000
	−1.0105	−0.9479	−0.8705	−0.822	−0.7400	0.985	667
Coordination number, Z	14.12	13.64	13.81	13.92	14.02	0.995	2000
	14.07	13.64	13.78	13.98	14.09	0.990	1000
	14.21	13.68	13.74	14.00	14.04	0.985	667
$U_{pot}/6NU_Az$	−1.0244	−0.9514	−0.8809	−0.8411	−0.8020	0.995	2000
d_0/d_{AA}	14.90	13.75	13.61	13.49	13.38	0.995	2000
	0.9677	0.9917	1.0084	1.0178	1.0255	0.995	2000

amorphous systems. The temperature of the system is defined according to the equipartition principle by the time average of the kinetic energy, $\langle U_{kin} \rangle = \frac{3}{2}kT$.

The amorphous system is generated in the following way. First, N randomly positioned hard spheres with radius r_{min} are filled into the periodicity cube. If $r_{min} = 0.39(V/N)^{1/3}$ is chosen, this requires about $5.4N$ trials. The first N_B of these are interpreted as B-type atoms and the remaining ones as A-type atoms. These positions are then relaxed to a densely packed amorphous arrangement. The relaxation may be achieved by the static (zero-temperature) procedure described by Brandt and Kronmüller (1987); this uses first merely repulsive potentials at fixed volume and then switches on the final potentials and relaxes the volume (pressure-free system). If desired, random atomic displacements with an amplitude decreasing with time may be added, which simulate finite temperature.

For the present simulations a dynamic relaxation method was preferred. This is more straightforward but slightly more time-consuming and yields practically the same fully relaxed atomic arrangements. With the correct potentials switched on, the initially nearly random positions are slowly annealed in a molecular-dynamics simulation. Cooling is achieved by reducing all velocities by a factor $C_{vel} = 0.995$ after each iteration step of length $dt = 0.007$ (in our reduced units $\hat{t}$). After 2000 time steps the system is practically fully relaxed. This is checked by subsequent static relaxation, which converges after 10 to 50 steps and reduces the energy U_{pot} by a relative amount less than 5×10^{-5}. Faster annealing ($N_{rel} \geqslant 500$ steps with velocity reduction factors $C_{vel} \geqslant 0.98$) yields fully relaxed amorphous systems, too, but typically with slightly higher potential energy (table 1). After slow annealing, any set of $N = 1000$ random positions yielded amorphous states which, for the same atomic interaction and composition, exhibit energies that differ very little (table 1) and radial density functions that practically coincide (§ 3).

Our molecular-dynamics simulation uses the velocity form of the Verlet algorithm (Swope *et al* 1982) to integrate the Newton equations for each atom. This algorithm proves numerically very stable and allows one to choose large time steps, even with single accuracy, thus saving computation time. We chose the time step dt to be so large that no more than a few atoms move more than $0.05d_{AA}$ in one step. This means $dt = 0.004$ to 0.007 depending on the temperature.

A feeling for the required time step is provided, for example, by the oscillation frequency ν of a B-type atom interacting with 12 A-type atoms situated at a distance d_{AB}. Averaging the curvatures of the 12 potentials ϕ_{AB} over all orientations yields the curvatures of the potential well (the spring constant) $k = 12\langle\cos^2\varphi\rangle \phi''_{AB}(d_{AB}) = 4\phi''_{AB}(d_{AB})$ and thus the oscillation frequency

$$\nu = (1/2\pi)(k/m)^{1/2} = (1/\pi)[\phi''_{AB}(d_{AB})/m_B]^{1/2}. \tag{5}$$

For example, with $\phi_{AB} = \phi_2$, $a_{AB} = 1$, $d_{AB} = 0.8$, $R_{AB} = 1.1$ and $m_B = 0.25$ one gets $\phi''_{AB}(d_{AB}) = 8(R_{AB} - d_{AB})^{-2} = 88.9$ and $\nu = 6.00$. Thus $(\nu\,\mathrm{d}t)^{-1} \simeq 24$ time steps of length 0.007 occur during one oscillation period.

When desired, the volume of the model was relaxed such that there is no applied pressure during the molecular-dynamics calculation. This was achieved by carefully relaxing the ratio of the periodicity length and the width d_{AA} of the potential ϕ_{AA} in each time step. We do this by formally changing the length scale of the potentials while leaving the periodicity volume and the atomic positions unchanged. For improved stability the relative change of this length is restricted to 1% per time step. This formal change of d_{AA} should not be confused with the fact that our final results are presented with d_{AA} as length unit. For the relaxation of the volume the sums of the first and second derivatives of U_{pot} with respect to the r_{ij} have to be calculated in each time step.

A convenient measure for the density of the atomic arrangement is the atomic spacing $d_0 = 2^{1/6}(V/N)^{1/3}$ of an FCC lattice with the same atomic density. The ratio d_0/d_{AA} is just the ratio by which the linear extension of the system changes when pressure is applied or when the volume is relaxed. Our relaxation always started with the FCC density, $d_0/d_{AA} = 1$. After annealing, i.e. when zero temperature was reached, d_0/d_{AA} attained an equilibrium value slightly larger or smaller than 1 (cf. table 1). That a seemingly larger equilibrium density than in the ideal FCC lattice is possible in amorphous arrangements, namely when $d_0 < d_{AA}$, simply reflects the fact that in our model the atomic radius is not prescribed as rigorously as for hard spheres. Some atomic pairs have distances less than d_{AA} as may be seen from the radial density functions in § 3.

3. Radial density functions

In figures 2 to 5 normalised radial density functions $g(r)$ are plotted for fully relaxed systems of 1000 atoms:

$$g(r) \equiv 4\pi r[\rho(r)/\rho(\infty) - 1] \tag{6}$$

where $\rho(r)$ is the radial density. The partial density functions $g_{AA}(r)$, $g_{AB}(r)$ and $g_{BB}(r)$ are defined by counting only the A–A, A–B or B–B atomic pairs, and $g_{tot}(r)$ by counting all atoms (cf. e.g. Brandt and Kronmüller 1987). The scale of the ordinate in figures 2 to 5 is fixed by the condition that $g(r) = -4\pi r$ must hold for small r (and for all distances where $\rho(r) = 0$; see figure 12 below). The depicted smooth $g(r)$ are obtained by the convolution of the original histogram $g_i \simeq g(r_i)$ ($r_i = i\Delta r$, $\Delta r = 1/80$) by a Gaussian of width $\delta = 0.048$:

$$g(r) = (2\pi\delta^2)^{-1/2} \sum_i g_i \exp[-(r - r_i)^2/\delta^2]. \tag{7}$$

Figure 2 shows $g(r)$ for systems consisting of only one type of atom interacting by potentials $\phi = \phi_2(r)$ (cf. the curve ϕ_{AA} in figure 1) with ranges $R = 1.2, 1.3, 1.4$ and 1.5. With increasing hardness of the potential, i.e. with decreasing R, the first peak in $g(r)$

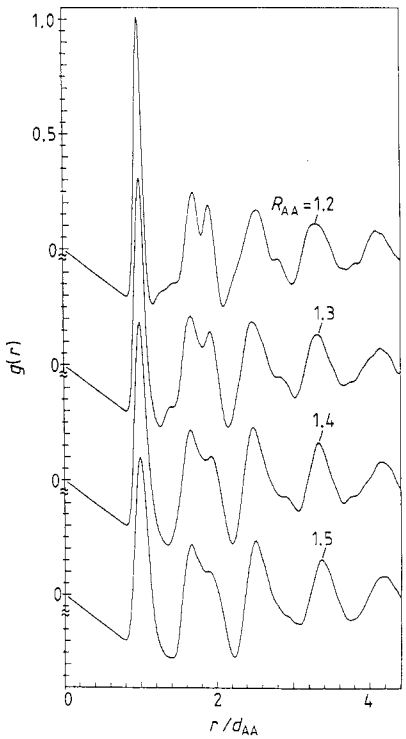

Figure 2. Radial density functions of one-component systems of $N = 1000$ atoms interacting by the Lennard-Jones-type potentials $\phi_2(r)$, equation (1), for various ranges $R_{AA}/d_{AA} = 1.2$ to 1.5 (see text). The scale for $g(r)$ is $0.02/d_{AA}$ in all plots of $g(r)$ in this paper.

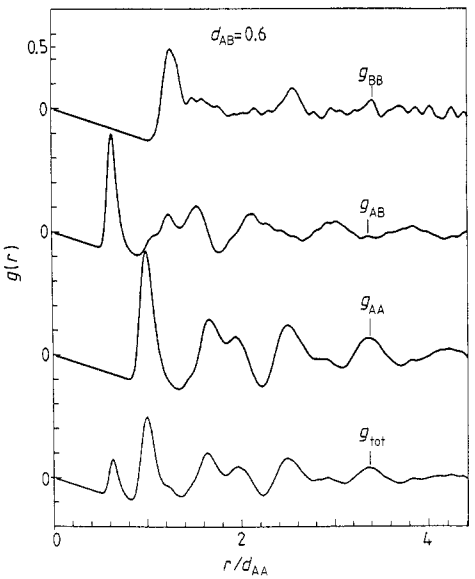

Figure 3. Partial radial density functions for $N_A = 800$ large and $N_B = 200$ small atoms, $d_{AB} = 0.6$, $r_B/r_A = 0.2$ (see text).

becomes sharper and the splitting of the second peak, the first and second minima, and the hump to the left of the minimum become more pronounced. The large coordination numbers $Z \simeq 14$ (number of nearest neighbours) listed in table 1 are defined by integrating the first peak in the radial density $\rho(r)$ up to the first minimum occurring at $r \simeq 1.4$ in figure 2. Note that at this minimum $\rho(r)$ is very small, in contrast to the FCC lattice which has a peak at $r = \sqrt{2}$.

In the computation of figure 2 the volume was not relaxed. After relaxation of the volume practically the same functions $g(r)$ are obtained. The change d_0/d of the linear extension of the system during this pressure-free relaxation is given in table 1.

Figures 3 to 5 show the partial density functions for systems of 800 A-type and 200 B-type atoms. In figure 3 ($d_{AB} = 0.6$) and figure 4 ($d_{AB} = 0.75$) the B-type atoms are smaller than the A-type atoms and in figure 5 ($d_{AB} = 1.3$) they are larger. The other parameters of the potentials are for figures 3, 4 and 5, respectively, $\phi_{AA} = \phi_2$, $R_{AA} = 1.4$ (1.4, 1.5), $\phi_{AB} = \phi_3$ (ϕ_2, ϕ_2), $a_{AB} = 1$, $R_{AB} = 1$ (1.25, 1.8), $\phi_{BB} = \phi_1$, $a_{BB} = 0.5$ (0.5, 1), $d_{BB} = 1$ (1, 1.2) and $R_{BB} = 1.4$ (1.4, 1.8).

The volume was not relaxed in figures 3 and 4; for small B-type atoms the volume relaxes only by a few per cent and the radial density is practically unchanged. For large B-type atoms, figure 5, the energy increases considerably when the volume is kept fixed at the FCC value of the A-type atoms. The volume was, therefore relaxed in figure 5; this increased the linear extension of the system by a factor of 1.155.

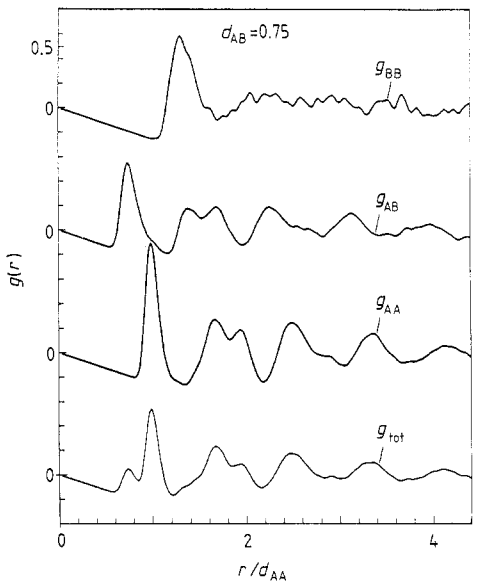

Figure 4. As figure 3 but for $d_{AB} = 0.75$, $r_B/r_A = 0.5$.

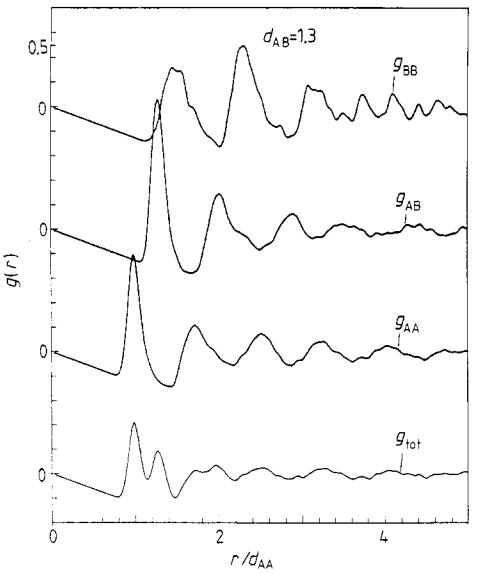

Figure 5. Partial radial density functions for $N_A = 800$ small and $N_B = 200$ large atoms, $d_{AB} = 1.3$, $r_B/r_A = 1.6$.

The partial density functions of this model were compared by Kizler (1988) and Kizler *et al* (1988) with those obtained for $Fe_{80}B_{20}$ by neutron and x-ray scattering. Good agreement was found. Kizler (1988) investigated also the distribution of the angles under which a given atom sees pairs of nearest neighbours in the present model and other models.

4. Atomic positions

Whereas radial density functions give quantitative but angular-averaged data, a better visualisation of the atomic arrangements is achieved by direct plots of the atomic positions. We choose the following presentation as a first trial. We cut our periodicity cube into parallel slices of equal thickness, project the atomic centres of each slice on a plane parallel to the slice, and draw circles of the corresponding atomic radii r_A or r_B around it. If a slice contains too few atoms there will be gaps between the circles, and if it contains too many the circles will overlap. But with appropriate choice of the number of slices and atoms the projected circles will look almost like a two-dimensional arrangement of discs with few overlaps and gaps, and still represent a three-dimensional atomic arrangement.

The following figures show such representations of equilibrium systems of 250 atoms with the periodicity cube cut into six slices. Slices with increasing height are represented in the sequence: lower left, lower right, middle left, middle right, upper left, upper right. The atomic centres are marked by crosses. The dash length of the circles indicates the height of the atoms; short (long) dashes mean that the atomic centre is close to the lower (upper) surface of the slice. This presentation in principle contains all information on the atomic positions. For better visualisation three such plots may be drawn for a given system, with cuts perpendicular to the x, y and z directions.

Each of the six squares in a plot has periodic boundary conditions, i.e. a circle cut by one boundary is supplemented at the opposite boundary. Note that in these plots many circles touch although the interaction is rather soft, i.e. the minima of ϕ_{AA} and ϕ_{BB} are wide, and although the presentation projects the atoms into planes.

In order to emphasise certain symmetry configurations, some of the circles are shown hatched and some atomic centres are connected by lines. This marking visualises that in amorphous metals and alloys the symmetry configurations in general are distorted. In particular, the polyhedra (or polygons in our plots) investigated by Bernal (1959) and Finney (1970) are not regular. This fact was particularly stressed by Egami *et al* (1980), Srolowitz *et al* (1981) and Chen *et al* (1988): the *distortion* of a polyhedron turns out to influence the point shear stress at the atom in its centre more than does the *type* of polyhedron. Symmetry considerations in amorphous systems, therefore, have to be taken with care.

The purpose of these plots is to indicate the influence of the interaction potentials on the atomic structure and to stimulate new ideas as to what might be the meaning and position of the 'free volume' and the two-level systems (Anderson *et al* 1972, Kronmüller 1983, Chen 1986). They might further indicate possible relaxation mechanisms (Gibbs *et al* 1983) and possible diffusion paths. Though the present paper cannot answer all these questions it might help to pose the questions on the local structure and dynamics of amorphous alloys more clearly and show how to proceed further.

5. Relaxed random positions

Figures 6 and 7 show amorphous one-component systems ($N_B = 0$) with potential range $R_{AA} = 1.3$. Figure 8 shows the corresponding radial density $g(r)$. In figure 6 the interaction has a repulsive core and an attractive tail ($\phi_{AA} = \phi_2$) and in figure 7 it is merely repulsive ($\phi_{AA} = \phi_1$, volume kept constant). Note that the first peak and the splitting of the second peak are more pronounced for the Lennard-Jones-type potential, figure 6, which yields a coordination number $Z = 13.92$. For the repulsive potential, $Z = 14.10$ is slightly larger, probably since the energy barriers for rearrangements are lower for this smooth interaction. The shear modulus for such systems under pressure is small and even vanishes for certain smooth potentials, e.g. for a logarithmic potential in two dimensions (Brandt 1969, 1986).

The atomic arrangements look very similar in figures 6 and 7. There are quite a few almost regular pentagons and hexagons. In some cases their central atom can be seen in the same slice, in some it may be found in the slice above or below, and some pentagons exhibit no central atom and no atomic pair sitting close to the symmetry axis of the pentagon; these thus encircle a small hole. In general it is not easy to identify real holes in our representation since atoms that have their centres in the slice above or below may fill the seeming hole. Also the partial overlap of circles may be genuine, due to the softness of the interaction, or apparent as can be seen from the different dash lengths of circles belonging to atoms centred at different height.

The arbitrary lines connecting some of the atomic centres show that the lattice planes or rows are not well defined in such amorphous systems. Several nearly straight rows of touching atoms may be identified but these end (or leave this slice) after five to eight atoms. Slightly or strongly curved rows may be seen as well. The choice of such rows is not unique, in contrast to ideal or defective crystals.

Figure 9 shows an amorphous two-component system ($N_A = 200$, $N_B = 50$) with

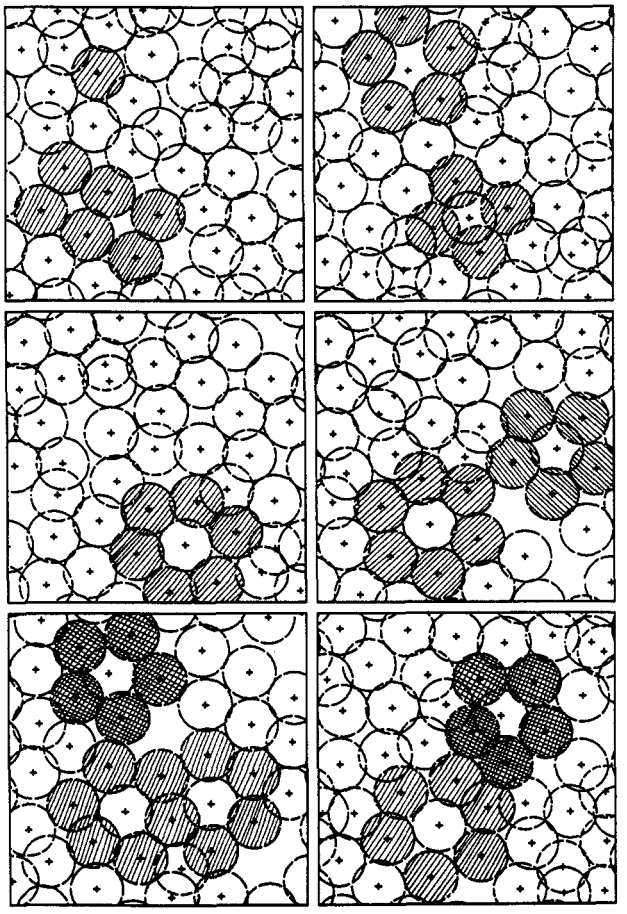

Figure 6. Atomic positions in an amorphous system of 250 atoms of one type interacting by a Lennard-Jones-type potential in a cube with periodic boundary conditions. The six squares show the atoms in six parallel slices (see text). Hatching is only a guide to the eye.

'hard' interaction ($R_{AA} = 1.3$) and $\phi_{AA} = \phi_{AB} = \phi_3$, $a_{AB} = 2$, $d_{AB} = 0.8$, $R_{AB} = R_{AA} = 0.2$, $\phi_{BB} = \phi_1$, $a_{BB} = 0.5$, $d_{BB} = 1$, $R_{BB} = R_{AB}$ and volume = constant. The ratio of the radii is $r_B/r_A = 2d_{AB} - 1 = 0.6$. The radial density for this system looks similar to that in figure 3 but its peak is slightly more pronounced since the interaction is shorter-ranged. Owing to the presence of two atomic sizes in figure 9, fewer configurations of high symmetry occur than in figures 6 and 7 and these are typically more distorted. Some of the small atoms form the centre of a pentagon of big atoms. In our alloys more empty space occurs than in one-component systems because the small atoms require less space but the big atoms cannot relax sufficiently to compensate for this. The volume was not relaxed in figures 6 and 7, but with volume relaxation practically identical figures result.

The arrangements for different ranges $R_A = 1.3$ to 1.5 look similar. Only when potentials with unphysically short range are used ($R_{AA} \leq 1.2$, 'sticking hard spheres') does the picture differ markedly; in this case more 'microcrystals' occur and more holes, and the atomic density now fluctuates more since a higher energy is required to rearrange atoms. On the other hand, very soft potentials do not yield a markedly different picture than that shown in figure 9, even merely repulsive potentials under pressure.

Figure 10 ($N_A = 200$, $N_B = 50$) shows an amorphous system with large B-type atoms ($d_{AB} = 1.3$, $r_B/r_A = 2d_{AB} - 1 = 1.6$, all potentials as in figure 5). The volume was relaxed; this resulted in a linear extension of 1.155 as in figure 5. Obviously, alloying

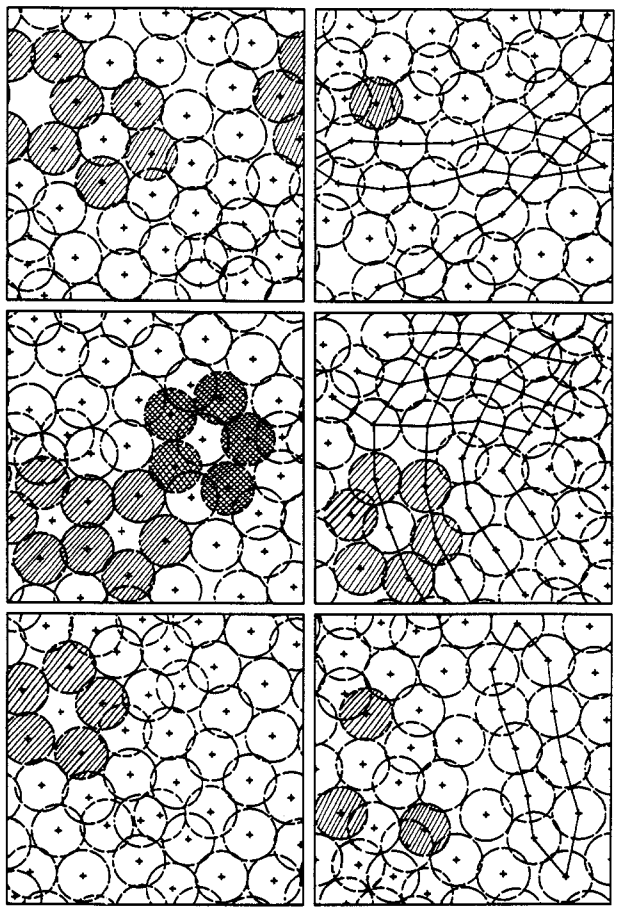

Figure 7. As figure 6 but for a merely repulsive potential under pressure. The lines connecting the atomic centres are guides to the eye.

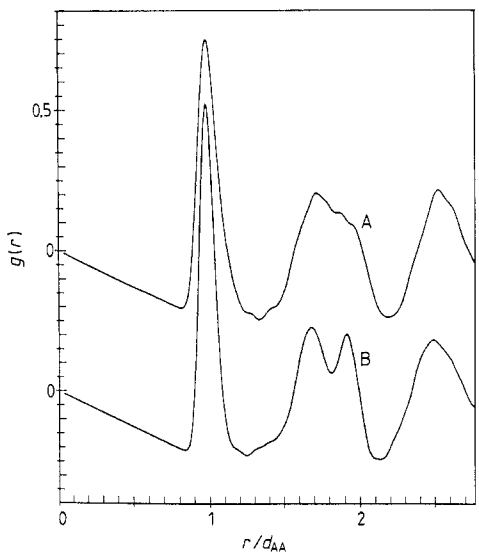

Figure 8. The radial density functions of the amorphous systems of figures 6 and 7: curve A, repulsive interaction (figure 7); curve B, interaction with repulsive core and attractive tail (figure 6).

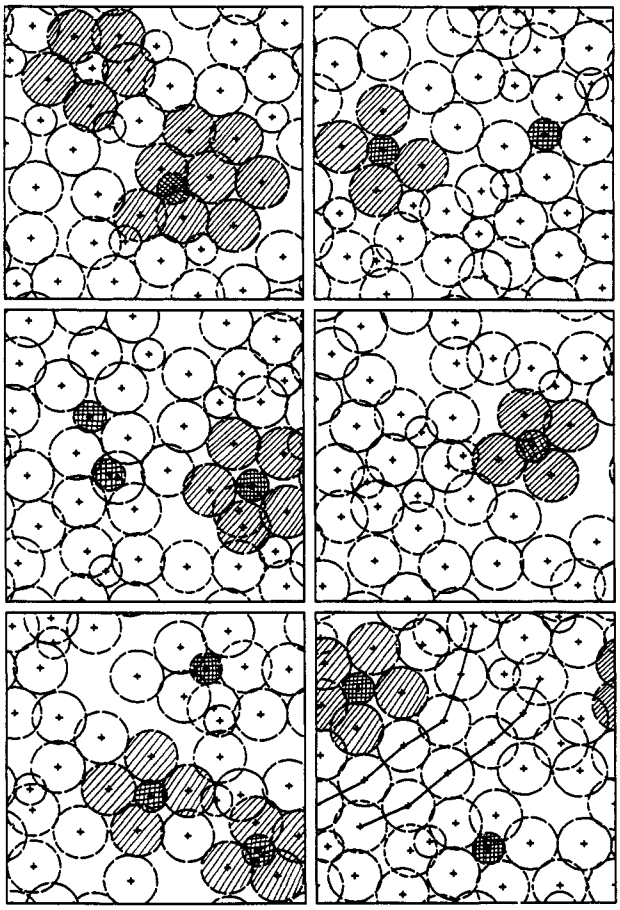

Figure 9. Amorphous two-component system of $N_A = 200$ large and $N_B = 50$ small atoms ($r_B/r_A = 0.6$) with hard interaction ($R_{AA} = 1.3$).

with a small amount of big atoms perturbs the system more than small atoms do. Some of the large atoms are surrounded by a ring of eight small atoms. Somewhat unexpectedly, no big holes occur. All seeming gaps are filled with one or two big atoms which have their centre in the slice above or below. One may say that the small (majority) atoms effectively fill the gaps between the big atoms. Note also that many circles touch even though the interaction in figure 10 is rather soft.

6. Amorphisation of defective crystals

During our computer simulation amorphous crystals never crystallised. In fact, the better the relaxation was, the 'more amorphous' became the system, viz. the radial density deviates more from that of perturbed crystals. In particular, the minimum near $r/d_{AA} \simeq 1.4$ (the position of the second peak in the FCC lattice) gets deeper and $\rho(r)$ becomes almost zero there. Apparently crystallisation requires a sufficiently large nucleus or surface that is already crystalline. Starting at sufficiently high temperature our slow annealing method always yields the same amorphous equilibrium arrangement in the sense that, for the same composition and interactions, the slightly smoothened radial density functions practically coincide and do not depend on the starting configuration. This is not true for careful static relaxation methods. These may yield

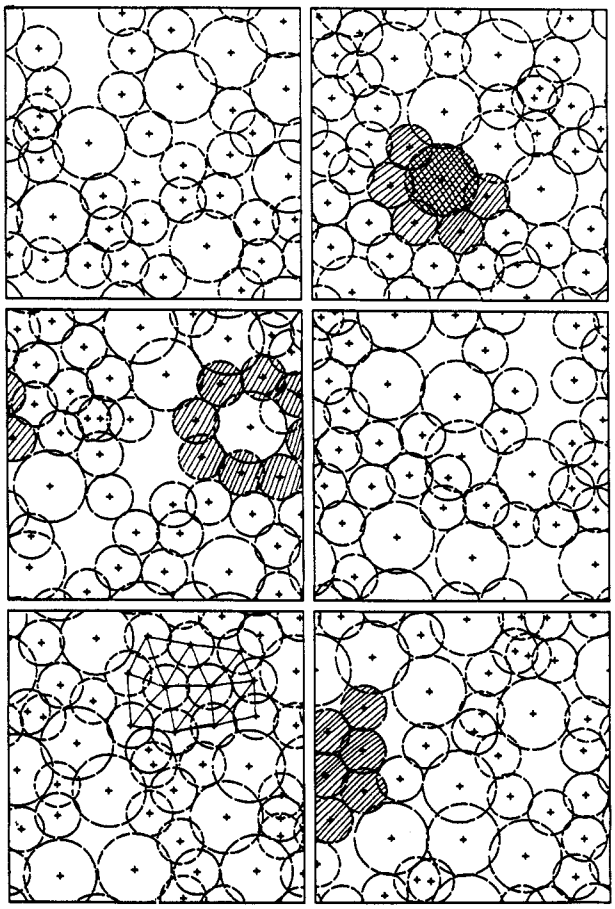

Figure 10. Amorphous two-component system of $N_A = 200$ small and $N_B = 50$ large atoms ($r_B/r_A = 1.6$, same potentials as in figure 5).

metastable amorphous systems which exhibit regions of lower-than-average density (Brandt 1984).

In order to get more insight into the way this randomisation occurs, we performed simulations starting with a defective crystalline arrangement of atoms, which was then annealed at various velocities. Some of the results are shown in figures 11 to 13 for an FCC lattice of originally 256 A-type atoms from which six are taken away, thus creating six vacancies at random positions, and then 50 atoms are replaced by smaller ones (B-type) of which 25 are randomly positioned and 25 are neighbours, thus creating a hole. The resulting starting configuration exhibits $N_A = 200$ and $N_B = 50$ as in figure 9.

In figure 11 the potentials are as in figure 9 ($R_{AA} = 1.3, R_{AB} = R_{AA} - 0.2, d_{AB} = 0.8$, thus $r_B/r_A = 0.6$) but with weaker A–B interaction, $a_{AB} = 1$. The molecular dynamics started with the perturbed FCC lattice, then annealing was performed by reducing all velocities by a factor 0.985 in each time step ($dt = 0.007$). Note the big hole, which is real, as can be seen by cutting along different directions. Large parts of the system remain crystalline with defects; thus the annealing in this case did not change the arrangement qualitatively. The smaller atoms sit in vacancies or holes but in general are not centred in these but preferably stick to internal surfaces.

The radial density of this relaxed defective crystalline system exhibits rather narrow lines (figure 12). The lines of $g_{AA}(r)$ are typical for the FCC lattice (at $r = 1, \sqrt{2}, \sqrt{3}, 2,$

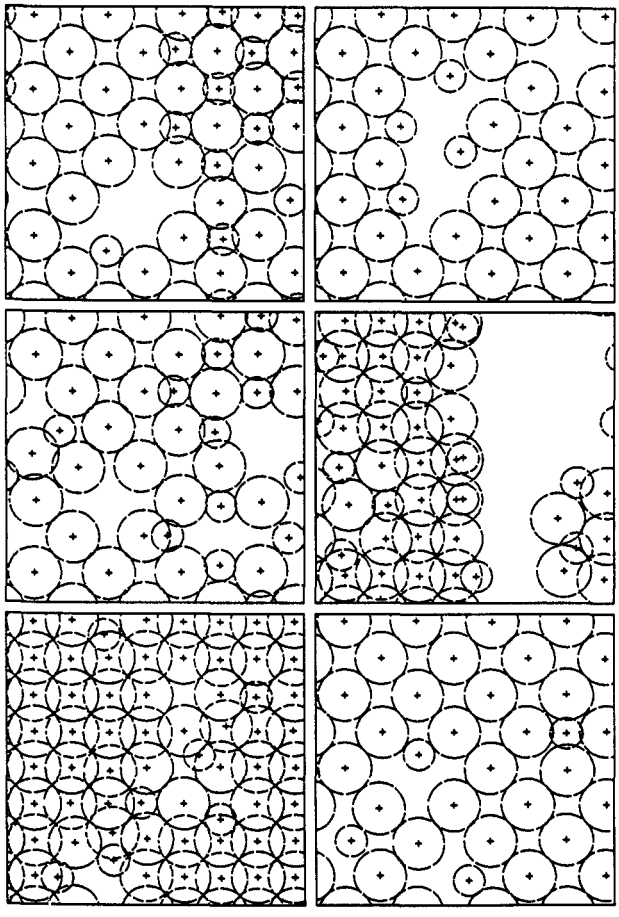

Figure 11. Relaxed defective crystal with initially six random vacancies, 25 randomly chosen large atoms replaced by small atoms, and 25 neighbouring atoms replaced by small ones. $N_A = 200, N_B = 50$ as in the amorphous system of figure 9. Hard interaction ($R_{AA} = 1.3$).

$\sqrt{5}$, etc.). In $g_{AB}(r)$ only the line at $r = 0.8 = d_{AB}$ is pronounced, and $g_{BB}(r)$ just reflects the strong repulsion which we assumed for the B-type atoms. The smearing of the lines in figure 12 is due to lattice distortions caused by relaxation around defects. Note, however, that for systems consisting of only one type of atom no relaxation occurs around vacancies if the range of their interaction is $R_{AA} \leqslant \sqrt{2}$. In this case only nearest neighbours interact in ideal FCC, HCP or BCC lattices and therefore the *force* between each pair of atoms is exactly zero, not only the *sum* of the forces on each atom. Thus the system will remain in static equilibrium if one or several atoms are taken away.

From this argument we conclude that *relaxation around a vacancy occurs only when the range of the interaction extends beyond the nearest neighbours*, or when the potentials are not rotationally symmetric or are not pair potentials, or if external pressure is applied. In this latter case the atoms do not sit in the potential minima of their neighbours. A further possibility for relaxation to occur is when atoms of different interaction are present. This is the case in figures 11 and 12. As a result the distances between neighbouring type-A atoms are not all exactly d_{AA} and therefore the peaks in $g_{AA}(r)$ are slightly smeared.

An interesting effect occurs when the interaction is chosen to be softer. Beyond a certain value of the 'softness' R_{AA} the annealing of a defective FCC lattice suddenly yields an amorphous system. This 'amorphisation' is shown in figures 13 and 14 for exactly the same starting configuration as in figures 11 and 12, and for the same annealing method and

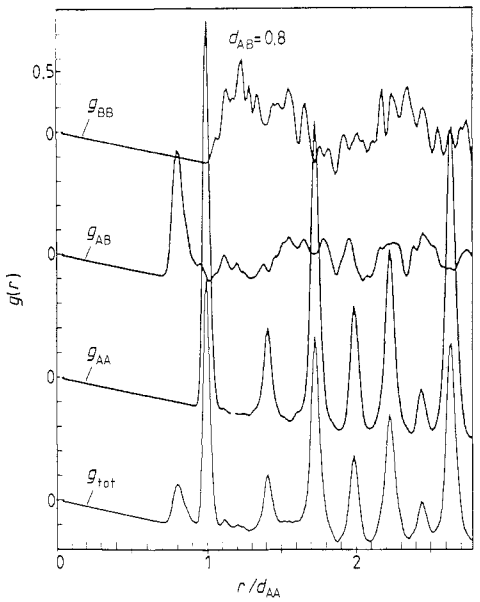

Figure 12. Partial radial density function for the system of figure 11. The distribution $g_{AA}(r)$ of the A-type atoms looks as expected for a distorted FCC lattice. Note the peak at $r = 1.4\, d_{AA}$ which is absent in BCC crystals and in relaxed amorphous systems.

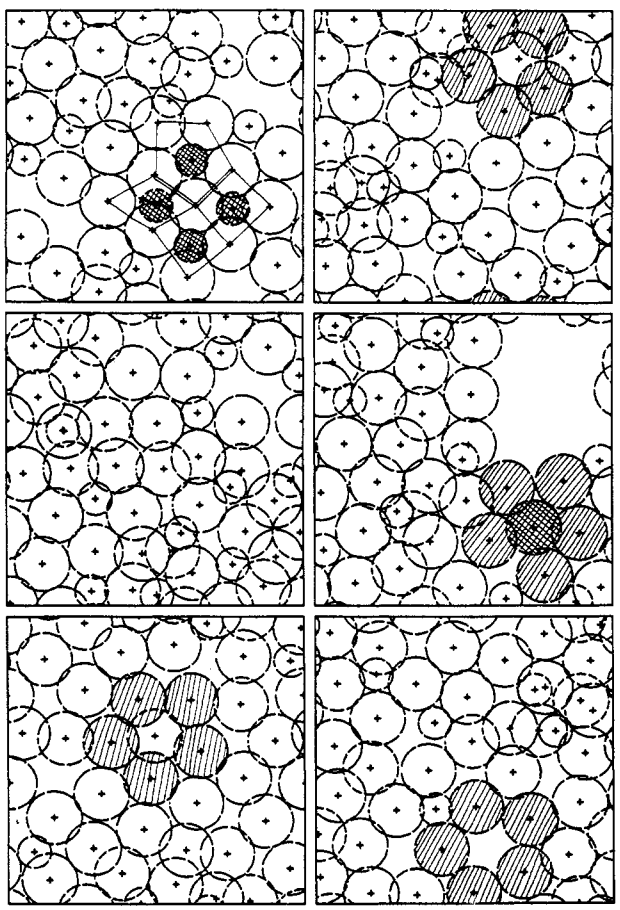

Figure 13. Amorphous system generated by the relaxation of the same initial configuration as in figure 11 (defective FCC crystal), with identical annealing rate but with slightly softer interaction of the atoms ($R_{AA} = 1.4$ rather than 1.3). This small difference leads to a completely different arrangement which, apart from the existence of a big hole, cannot be distinguished from other amorphous systems generated by relaxation of random positions, cf. the radial densities in figures 12 and 14.

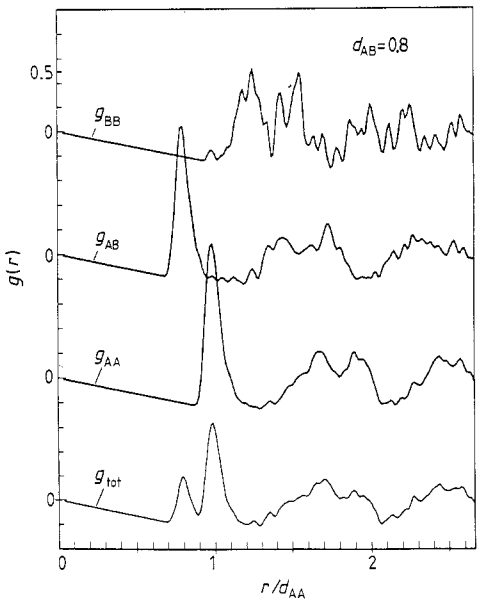

Figure 14. Partial radial density functions for the system of figure 13. As compared with figure 12 the system is now completely amorphous. In particular, $g_{AA}(r)$ no longer has a peak at $r = 1.4\ d_{AA}$ but rather a minimum and looks like the $g_{AA}(r)$ in figure 4.

presentation but for $R_{AA} = 1.4$ instead of $R_{AA} = 1.3$. The resulting atomic arrangement (figure 13) looks similar to that in the amorphous systems in figure 9, and the radial density (figure 14) looks as in figures 3 or 5. In particular, there are several almost regular pentagons in the arrangement, and the line at $r = 1.4$ in $g(r)$ has disappeared completely. The only relict of the original defective FCC lattice is a hole at the same position as in figure 11. This means that without applied pressure holes do not tend to collapse in our model system.

The observed transition to a fully amorphous arrangement when R_{AA} is changed clearly depends on the relaxation method. For example, careful static relaxation still yields defective crystals at even softer potentials, and very long dynamic relaxation, which keeps the system at high temperature for a while, will yield an amorphous system at harder potentials. Anyway, this finding indicates that small differences in the interaction potential may lead to a completely different system after relaxation and that after amorphisation of a defective lattice the short-range order may be lost completely but holes or internal surfaces may survive.

The presence of such stable cracks, channels or holes may be of importance for self-diffusion in amorphous systems. Their existence, size, geometry, etc., in real systems should be investigated by appropriate experiments in order to facilitate the interpretation of diffusion measurements. Our computer simulation of self-diffusion (part II) so far is restricted to quite dense and well relaxed systems at relatively high temperatures. The simulation of diffusion in not fully relaxed systems requires lower temperatures to avoid further relaxation before the atoms have diffused markedly. Such simulations are very time-consuming.

7. Summary

Completely relaxed amorphous systems containing one or two types of atoms interacting by rotationally symmetric pair potentials with repulsive core and attractive tail are usually dense and free of easily visible holes or channels. If the simulated annealing is

performed too fast, the resulting amorphous arrangement is less compact but real holes or dilute regions still cannot be seen in our plots. Metastable density fluctuations can be detected in this case by more subtle averaging methods (Brandt 1984, Lakkonen and Nieminen 1988).

Holes and regions with 'free volume' are observed in simulations with extremely short-ranging potentials ('magnetic' hard spheres) or when crystals containing a sufficient concentration of defects are annealed at sufficiently low temperature and with not too long-ranging potentials. On the other hand, the most homogeneous amorphous systems (with least density fluctuations and no holes) are obtained for merely repulsive interaction under pressure. In this case the density cannot be compared with that of hard spheres since the atomic radius is not defined.

Annealing at higher temperatures always results in amorphous arrangements that have no memory of the original atomic arrangement. After complete relaxation the same partial density functions were always obtained whatever the initial position of the atoms.

All our simulated amorphous systems exhibit complete absence of real microcrystallites. In the plots of the atomic positions some hexagons occur, in particular in systems with one type of atom, but these hexagons are more or less distorted. Distorted also are the lattice planes, which may be drawn in these plots in a quite arbitrary way. A further indication of a completely amorphous state is that many pentagons can be seen in these plots.

In conclusion, inspection of the static equilibrium arrangement of atoms does not give a clear indication of preferred diffusion mechanisms. More informative will be the plots of diffusion paths presented in part II or plots of correlated motion, which are in preparation.

Acknowledgments

I thank sincerely C Esparza, W Frank, J Horváth, H Kronmüller and G Tichy for helpful discussions.

References

Ackland G J, Tichy G, Vitek V and Finnis M W 1987 *Phil. Mag.* A **56** 735
Anderson P W, Halperin B I and Varma C M 1972 *Phil. Mag.* **25** 1
Bernal J D 1959 *Nature* **183** 141
Brandt E H 1969 *Phys. Status Solidi* **35** 1027
—— 1984 *J. Phys. F: Met. Phys.* **14** 2485
—— 1985 *Cryst. Latt. Defects Amorph. Mater.* **11** 171
—— 1986 *Phys. Rev.* B **34** 6514
—— 1989 *J. Phys.: Condens. Matter.* **1** 10003
Brandt E H and Kronmüller H 1983 *Phys. Lett.* **93A** 344
—— 1987 *J. Phys. F: Met. Phys.* **17** 1291
Chen H S 1986 *Amorphous Metals and Semiconductors* ed. P Haasen and R I Jaffee (Oxford: Pergamon)
Chen S-P, Egami T and Vitek V 1988 *Phys. Rev.* B **37** 2440
Daw M S and Baskes M I 1983 *Phys. Rev. Lett.* **50** 1285
—— 1984 *Phys. Rev.* B **29** 6443
Egami T, Maeda K and Vitek V 1980 *Phil. Mag.* A **41** 883
Finney J L 1970 *Proc. R. Soc.* A **319** 479, 495
Finnis M W and Sinclair J E 1984 *Phil. Mag.* A **50** 45
Frank W, Horváth J and Kronmüller H 1988 *Mater. Sci. Eng.* **97** 415

Gibbs M R J, Evetts J E and Leaky J A J 1983 *J. Mater. Sci.* **18** 278
Horváth J, Ott J, Pfahler K and Ulfert W 1988 *Mater. Sci. Eng.* **97** 409
Horváth J, Pfahler K, Ulfert W, Frank W and Kronmüller H 1987 *Mater. Sci. Forum* **15** 523
Kizler P 1988 *Thesis* Universität Stuttgart
Kizler P, Lamparter P and Steeb S 1988 *Mater. Sci. Forum* **97** 169
Kronmüller H 1983 *Phil. Mag.* B **48** 127
Kronmüller H, Fähnle M, Domann M, Grimm H, Grimm R and Gröger B 1979 *J. Magn. Magn. Mater,* **13** 53
Kronmüller H and Frank W 1989 *Radiation Effects and Defects in Solids* **108** 81
Kronmüller H and Ulner J 1977 *J. Magn. Magn. Mater.* **6** 52
Laakkonen J and Nieminen R M 1988 *J. Phys. C: Solid State Phys.* **21** 3663
Piller J and Haasen P 1982 *Acta Metall.* **30** 1
Seeger A 1955 *Handbuch der Physik* vol. VIII, 1 (Berlin: Springer)
—— 1958 *Handbuch der Physik* vol. VIII, 2 (Berlin: Springer)
Srolowitz D, Maeda K, Vitek V and Egami T 1981 *Phil. Mag.* A **44** 847
Swope W C, Andersen H C, Berens P H and Wilson K R 1982 *J. Chem. Phys.* **76** 637
Wördenweber R, Pruymboom A and Kes P H 1988 *J. Low Temp. Phys.* **70** 253